0026-895X/08/7402-413–422$20.00
MOLECULAR PHARMACOLOGY
Copyright © 2008 The American Society for Pharmacology and Experimental Therapeutics
Mol Pharmacol 74:413–422, 2008

Vol. 74, No. 2
47209/3362572
Printed in U.S.A.

Spatial Approximation between Secretin Residue Five and the Third Extracellular Loop of Its Receptor Provides New Insight into the Molecular Basis of Natural Agonist Binding

Maoqing Dong, Polo C.-H. Lam, Delia I. Pinon, Patrick M. Sexton, Ruben Abagyan, and Laurence J. Miller

Department of Molecular Pharmacology and Experimental Therapeutics, Mayo Clinic, Scottsdale, Arizona (M.D., D.I.P., L.J.M.), Department of Molecular Biology, Scripps Research Institute and Molsoft LLC, La Jolla, California (P.C.-H.L., R.A.), and Department of Pharmacology, Monash University, Clayton, Victoria, Australia (P.M.S.).

Received March 12, 2008; accepted May 8, 2008

ABSTRACT

The amino terminus of class II G protein-coupled receptors plays an important role in ligand binding and receptor activation. Understanding of the conformation of the amino-terminal domain of these receptors has been substantially advanced with the solution of nuclear magnetic resonance and crystal structures of this region of receptors for corticotrophin-releasing factor, pituitary adenylate cyclase-activating polypeptide, and gastric inhibitory polypeptide. However, the orientation of the amino terminus relative to the receptor core and how the receptor gets activated upon ligand binding remain unclear. In this work, we have used photoaffinity labeling to identify a critical spatial approximation between residue five of secretin and a residue within the proposed third extracellular loop of the secretin receptor. This was achieved by purification, deglycosylation, cyanogen bromide cleavage, and sequencing of labeled wild-type and mutant secretin receptors. This constraint has been used to refine our evolving molecular model of secretin docked at the intact receptor, which for the first time includes refined helical bundle and loop regions and reflects a peptide-binding groove within the receptor amino terminus that directs the amino terminus of the peptide toward the receptor body. This model is fully consistent with the endogenous agonist mechanism for class II G protein-coupled receptor activation, where ligand binding promotes the interaction of a portion of the receptor amino terminus with the receptor body to activate it.

Class II guanine nucleotide-binding protein (G protein)-coupled receptors are an important family of potential drug targets that are activated by natural peptide ligands greater than 25 residues in length (Ulrich et al., 1998). All of these agonist ligands possess diffuse pharmacophoric regions, with critical residues spread throughout the length of the peptides. This provides the opportunity to define spatial approximation between such ligand residues and distinct residues within its receptor because ligand and receptor are normally bound to each other. It has been remarkable that probes incorporating photolabile residues throughout the pharmacophore of secretin-27, in positions 6, 12, 13, 14, 18, 21, 22, 23, and 26, each covalently labeled distinct residues that are restricted to the amino-terminal region of the secretin receptor, without labeling the receptor transmembrane core (Dong et al., 1999a,b, 2000, 2002, 2003, 2007; Zang et al., 2003). This was interpreted as suggesting that there is a peptide-binding platform within the amino-terminal domain of this receptor (Dong et al., 2006). To date, only probes with photolabile residues at the amino terminus of secretin have covalently labeled the receptor core (Dong et al., 2004a).

This has not provided adequate constraints to meaningfully align the receptor amino-terminal domain with the receptor core region in a molecular model of the intact secretin receptor. An initial attempt at this was recently performed based on a limited set of observations, including the proposed spatial approximation between a motif within the receptor amino terminus and its third extracellular loop region (Dong et al., 2006). That model was further tested and was compared with models incorporating two alternative orientations

This work was supported by National Institutes of Health grant DK46577 (to L.J.M.), National Health and Medical Research Council of Australia (NHMRC) project grant 436780 (to P.M.S.), and by the Fiterman Foundation. P.M.S. is a Principal Research Fellow of the NHMRC.

Article, publication date, and citation information can be found at http://molpharm.aspetjournals.org.

doi:10.1124/mol.108.047209.

ABBREVIATIONS: FRET, fluorescence resonance energy transfer; Bpa, *p*-benzoyl-L-phenylalanine; CNBr, cyanogen bromide; PMSF, phenylmethylsulfonyl fluoride; STI, soybean trypsin inhibitor; CHO-SecR, rat secretin receptor-bearing Chinese hamster ovary cell line; KRH, Krebs-Ringer/HEPES; ICM, internal coordinate mechanics; TM, transmembrane domain.

of these two secretin receptor domains reflecting recent reports of proposed orientations for other members of the class II G protein-coupled receptor family (Grace et al., 2004, 2007; Sun et al., 2007) in a report using quantitative fluorescence resonance energy transfer (FRET) analysis to establish the distances between residues at distinct sites within the docked secretin ligand and residues within each of the extracellular regions of the receptor (Harikumar et al., 2007). Although this provided a general validation of the molecular model of the secretin receptor that had been proposed (Dong et al., 2006), the large sizes of the fluorescence donors and acceptors that were used, their potential for disruption of normal structures, and the relatively long distances established in that work precluded detailed refinement of the molecular model. Subsequently, another higher resolution and more extensive crystal structure for the amino terminus of another class II G protein-coupled receptor, the receptor for gastric inhibitory polypeptide, was reported (Parthier et al., 2007). This provided opportunity for improved homology modeling of this important receptor domain.

In the current work, we have used intrinsic photoaffinity labeling with a secretin analog incorporating a *p*-benzoyl-L-phenylalanine (Bpa) moiety into position five to experimentally identify a new spatial approximation constraint between a key residue within the secretin pharmacophore and a residue within the third extracellular loop of the secretin receptor. This constraint turned out to represent a key new contribution to better establish the orientation of the ligand docked to the receptor amino terminus relative to the receptor core. These data have been used to generate an updated homology model of the receptor amino terminus and to further refine our evolving molecular model of the secretin-receptor complex. For the first time, we have refined the helical bundle and loop regions of this three dimensional molecular model. We have also used a new, more generalizable modeling approach that simultaneously applied the full battery of experimentally derived constraints to determine the best conformation now possible. We believe that this is fully consistent with all experimentally generated data to date and that it helps provide insights into a theme for peptide agonist ligand docking and activation of these receptors.

Materials and Methods

Materials. Cyanogen bromide (CNBr), the solid-phase oxidant *N*-chlorobenzenesulfonamide (iodobeads), and *m*-maleimidobenzoyl-*N*-hydroxysulfosuccinimide ester were purchased from Pierce Chemical Company (Rockford, IL). Phenylmethylsulfonyl fluoride (PMSF), 3-isobutyl-1-methylxanthine, and *N*-(2-aminoethyl-1)-3-aminopropyl glass beads were from Sigma-Aldrich Life Sciences (St. Louis, MO). Soybean trypsin inhibitor (STI) and tissue culture medium were from Invitrogen (Carlsbad, CA). Secretin and endoglycosidase F were prepared in our laboratory, as we have described previously (Pearson et al., 1987). All other reagents were of analytical grade.

Synthetic Peptides. The secretin-like probe, (Bpa^5,Tyr^{10})rat secretin-27 (Bpa^5 probe), was designed to incorporate a photolabile Bpa in position 5 to replace a threonine located within the amino-terminal half of the ligand and a tyrosine in position 10 to replace a leucine that has previously been shown to be well tolerated (Gardner et al., 1977; Kofod, 1991). This probe and another secretin analog to be used as a radioligand, (Tyr^{10})secretin, were synthesized using the procedures described previously (Powers et al., 1988). These peptides were radioiodinated oxidatively using 1 mCi of $Na^{125}I$ and exposure to the iodobead solid-phase oxidant for 15 s and were purified using reversed-phase high-performance liquid chromatography to yield specific radioactivities of 2000 Ci/mmol (Powers et al., 1988).

Receptor Sources. A Chinese hamster ovary cell line stably expressing the wild-type rat secretin receptor was used as source of receptor (CHO-SecR) (Ulrich et al., 1993). This cell line expresses approximately 12.5×10^4 receptor molecules per cell (M.D. and L.J.M., unpublished data). It was cultured at 37°C in a 5% CO_2 environment on tissue culture plasticware (Falcon; BD Discovery Labware, Bedford, MA) in Ham's F-12 medium supplemented with 5% Fetal Clone-2 (HyClone Laboratories, Logan, UT). Cells were passaged twice a week and lifted mechanically before use.

Two new secretin receptor mutants were prepared to introduce additional sites for CNBr cleavage in the fourth and seventh transmembrane segments (TM4 and TM7) of the receptor. These represented receptor constructs with His^{256} to Met (H256M) in TM4 and Leu^{360} to Met (L360M) in TM7. Both constructs were prepared using an oligonucleotide-directed approach with the QuikChange site-directed mutagenesis kit from Stratagene (La Jolla, CA), with the products verified by direct DNA sequencing (Sanger et al., 1977). They were expressed transiently in COS-1 cells (American Type Culture Collection, Manassas, VA) after transfection using a modification of the DEAE-dextran method (Holtmann et al., 1996). Cells were harvested mechanically 72 h after transfection.

A particulate fraction enriched in plasma membranes was prepared from the receptor-expressing cells using discontinuous sucrose gradient centrifugation (Hadac et al., 1996). Membranes were suspended in Krebs-Ringer/HEPES (KRH) medium (25 mM HEPES, pH 7.4, 104 mM NaCl, 5 mM KCl, 2 mM $CaCl_2$, 1 mM KH_2PO_4, and 1.2 mM $MgSO_4$) containing 0.01% STI and 1 mM PMSF, and were stored at −80°C until they were to be used in ligand binding and photoaffinity labeling studies.

Receptor Binding Studies. The Bpa^5 probe was characterized to test its ability to bind the secretin receptor. This was performed with membranes from the CHO-SecR cells in competition-binding assays, using conditions that have been previously established (Hadac et al., 1996). In brief, increasing concentrations of the Bpa^5 probe or secretin ranging from 0 to 1 μM were incubated with approximately 10 μg of membranes in the presence of a constant amount of the radioligand, (^{125}I-Tyr^{10})secretin (5–10 pM), in 500 μl of KRH medium containing 0.01% STI, 1 mM PMSF, and 0.2% bovine serum albumin for 1 h at room temperature. After the incubation, the membrane-bound radioligand was separated from free radioligand with a Skatron cell harvester (Molecular Devices, Sunnyvale, CA), using receptor-binding filtermats that had been presoaked in 0.3% hexadimethrine bromide. Bound radioactivity was quantified using a γ-spectrometer. Nonspecific binding was determined in the presence of 1 μM unlabeled secretin and represented less than 15% of total binding. Data were graphed using the Prism program (GraphPad Software, San Diego, CA) and were analyzed using the nonlinear least-squares curve-fitting program LIGAND (Munson and Rodbard, 1980). Analagous binding procedures were used to characterize binding of the H256M and L360M secretin receptor mutants expressed in COS-1 cells.

Biological Activity Assays. The Bpa^5 probe was characterized to test its ability to stimulate biological responses in secretin receptor-bearing CHO-SecR cells. This was studied by quantification of intracellular cAMP accumulation. For this, 50,000 cells per well were plated in 24-well plates and cultured for 72 h. Cells were washed twice with phosphate-buffered saline and stimulated for 30 min at 37°C with increasing concentrations of the Bpa^5 probe or secretin (0–1 μM) in 200 μl of KRH medium containing 0.01% STI, 0.2% bovine serum albumin, 0.1% bacitracin, and 1 mM 3-isobutyl-1-methylxanthine. The reaction was terminated by removing the peptide solution and adding 400 μl of 6% (w/v) ice-cold perchloric acid. After vigorous agitation for 15 min, the cell lysates were adjusted to pH 6.0 with 30% $KHCO_3$ and were cleared by centrifugation at 2000

rpm for 5 min. The supernatants were used for cAMP quantification in a [^{3}H]cAMP competition-binding assay using a kit from Diagnostic Products Corporation (Los Angeles, CA) per the manufacturer's instructions. Radioactivity was quantified by scintillation counting in a liquid scintillation counter (LS6000; Beckman Coulter, Fullerton, CA). Similar procedures used with COS-1 cells expressing the H256M and L360M secretin receptor mutants.

Photoaffinity Labeling. This was conducted using 50 μg of membranes and approximately 0.1 nM ^{125}I-labeled Bpa^5 probe in 500 μl of KRH medium containing 0.01% STI and 1 mM PMSF in the presence of increasing amounts of competing secretin. Incubations were performed for 1 h in the dark at room temperature and reactions were then exposed to photolysis for 30 min at 4°C using a Rayonet Photochemical Reactor (Southern New England Ultraviolet Co., Bradford, CT) equipped with 3500-Å lamps. After being washed twice with 1 ml of ice-cold KRH medium, membranes were solubilized in SDS sample buffer and component proteins were separated by gel electrophoresis on 10% SDS-polyacrylamide gels (Laemmli, 1970). Labeled products were visualized by autoradiography. The apparent molecular masses of radiolabeled bands were determined by interpolation on a plot of the mobility of ProSieve protein standards (Lonza Rockland, Rockland, ME) versus the log values of their apparent masses. Band densitometry was performed by the National Institutes of Health ImageJ software (http://rsb.info.nih.gov/ij/).

Analogous photoaffinity labeling procedures were also performed using membranes from COS-1 cells expressing the H256M and L360M secretin receptor mutants in the absence and presence of 1 μM competing secretin. For selected experiments, the affinity-labeled secretin receptor and its relevant fragments were deglycosylated with endoglycosidase F using the conditions described previously (Hadac et al., 1996).

CNBr Cleavage. For localization of regions and sites of covalent labeling, larger aliquots of receptor-bearing membranes, approximately 200 μg, and probe, approximately 0.5 nM ^{125}I-labeled Bpa^5 probe, were used. After electrophoresis, labeled receptor bands were excised from gels, eluted in water, lyophilized, and precipitated with 85% ethanol. Purified labeled receptor was solubilized in 60 μl of 0.1% SDS and digested with CNBr using conditions described previously (Dong et al., 1999b). For selected experiments, purified labeled receptor was deglycosylated with endoglycosidase F before CNBr cleavage. Products were separated on 10% NuPAGE gels (Invitrogen, Carlsbad, CA) using MES running buffer, and labeled bands were visualized by autoradiography. The apparent molecular masses of radiolabeled receptor fragments were determined by interpolation on a plot of the mobility of Multimark protein standards (Invitrogen) versus the log values of their apparent masses.

Radiochemical Sequencing. After achieving definitive identification of the receptor fragment that was labeled by the Bpa^5 probe, radiochemical sequencing was used to determine the specific receptor residue covalently labeled by the probe. For this, the labeled secretin receptor was purified and cleaved as described as above. The labeled Glu^{345}-Ile^{429} CNBr fragment from the wild-type secretin receptor was gel-purified to radioactive homogeneity before being covalently coupled through Cys^{367} to maleimidobenzoyl succinimide-activated *N*-(2-aminoethyl-1)-3-aminopropyl glass beads. Manual cycles of Edman degradation were repeated, as has been reported previously (Ji et al., 1997), and the radioactivity released in each cycle was quantified using a γ-spectrometer.

Molecular Modeling. All molecular modeling activities for this project were conducted using a stochastic global energy optimization procedure that has been implemented in internal coordinate mechanics (ICM) (Abagyan et al., 1994). This procedure consisted of three iterative steps: 1) random conformational change of a dihedral angle according to the biased-probability Monte Carlo method (Abagyan and Totrov, 1994); 2) local minimization of all free dihedral angles; and 3) acceptance or rejection of the new conformation based on the Metropolis criterion at the simulation temperature, usually at 600 K (Metropolis et al., 1953). This approach can generate and search through diverse sets of molecular conformations by actively sampling a selected set of dihedral angles. All calculations were carried out on 2.33 GHz Intel Dual Core XEON-EMT processors.

Conformations of the amino-terminal domain of the rat secretin receptor were determined by homology modeling, based on both the NMR distance constraints of the mouse CRF2β receptor amino-terminal domain that were recently deposited in PDB (Grace et al., 2007) and on the crystal structure of the amino terminus of the gastric inhibitory polypeptide receptor that was reported subsequently (Parthier et al., 2007). The latter was particularly important to add features such as the helical segment in the distal end of the receptor amino terminus that had not been well refined in the earlier NMR models. These structures were used as templates and constraints to generate an up-to-date static homology model of the structurally and functionally important amino-terminal domain of the secretin receptor. All side chains were sampled.

To build a model of the transmembrane helical bundle domain of the secretin receptor, we used the "cold-spot" method with the crystal structure of the human β2-adrenergic receptor as template (Cherezov et al., 2007). Because class I and II G protein-coupled receptors have clear differences in the positions and absence or presence of proline-induced kinks in their transmembrane helices, we tethered the intracellular sides of the helices up to the positions of the perceived differences, and the extracellular sides of the helices were allowed to pack themselves during the modeling process. The long modeling runs likely reflect the relative uncertainty in the positions of the extracellular sides of the helices. The three extracellular and three intracellular loops of the secretin receptor were subsequently built as full atomic models, with their ends tethered to a static copy of the helical bundle to maintain loop closure. The rest of the helical region was represented by grid maps. The backbone and side chains of the loops were then sampled on the grid representation of the transmembrane helical region. After simulation, a full atomic model of the transmembrane domain was constructed by connecting the helical bundle with the loops in one continuous chain. The 100 best energy conformations were retained and used in subsequent simulations.

The initial conformation of secretin to be used in docking was taken from a previous solution-phase NMR determination of the porcine secretin structure (Clore et al., 1988), with Arg^{14} modified to Gln^{14}, the residue present in this position in rat secretin. All side chains were sampled and minimized.

Docking of the Amino-Terminal Domain of the Secretin Receptor to the Transmembrane Domain of the Secretin Receptor. The carboxyl-terminal tail of the amino-terminal domain of the secretin receptor was tethered to a static copy of the top of TM1 of this receptor. A pentasaccharide $Man_3GlcNAc_2$ was attached to Asn^{50} to mimic its *N*-linked glycosylation state. A loose distance restraint was set between the WDN sequence and the top of the transmembrane domain. The amino-terminal domain was then docked to the grid representation of the transmembrane domain by Monte Carlo sampling of the six positional variables and minimization of all the side chain variables. For each of the 100 initial transmembrane domain conformations, 100 diverse amino-terminal domain docking poses were generated. These docking poses were evaluated by ICMPocketFinder (An et al., 2005). The conformations containing a small molecule/peptide binding pocket having the largest volumes and shortest distances to the photoaffinity labeled residues were selected. A total of 100 full receptor conformations were retained for peptide docking.

Docking of the Secretin Peptide to the Full Secretin Receptor. The secretin peptide was first docked to the grid representation of the full receptor in the presence of 10 distance restraints set between the C_β of the secretin peptide and the amino-terminal domain: peptide His^1 to receptor Phe^{338}, Thr^5 to Phe^{349}, Phe^6 to Val^4, Arg^{12} to Val^6, Leu^{13} to Val^{103}, Arg^{18} to Arg^{14}, Arg^{21} to Arg^{15}, Leu^{22} to Leu^{17}, Leu^{23} to Arg^{21}, and Leu^{26} to Leu^{36}. The peptide/receptor complex was then refined by treating the receptor as a full atomic/

grid representation hybrid model: 1) The amino-terminal domain was represented by full atomic model with flexible backbone and side chain. 2) The three extracellular loops of the transmembrane domain were represented by full atomic models with flexible backbone and side chains. The ends of each of the loops were tethered to the top of the helices. 3) The tops of the helices were represented by full atomic models with fixed backbone and flexible side chains. 4) The rest of the transmembrane domain was represented by grid maps.

In each refinement, the receptor amino-terminal domain was first truncated to include only residues from Arg^{9} to Arg^{112}. Arg^{112} was tethered to the top of TM1 to maintain closure. We did not use the previously reported spatial approximation constraint between Gln^{14} in the peptide and Pro^{38} in the receptor, because that had been established with a *p*-benzoyl-benzoyl-L-lysine photolabile moiety that is larger and more distant from the normal peptide backbone than the Bpa moiety and that the efficiency of covalent attachment with this probe was less than 1% of that observed with all the other probes (Dong et al., 2003). In addition, a subset of 300 NMR restraints of the CRF2β receptor amino-terminal domain was imposed on the residues that are conserved between the secretin receptor and the CRF2β receptor.

The secretin peptide/receptor complex was refined by progressive sampling of the positional variables of the peptide and the receptor amino-terminal domain, the backbone variables of the receptor extracellular loops and Gly^{34}-Cys^{44} of the receptor amino-terminal domain, followed by sampling of all side chain variables of the system. Subsequently, the highly flexible Ala^{1}-Pro^{8} segment of the receptor amino-terminal domain was built back into the model. The backbone and side-chain conformations of this flexible region were sampled.

Finally, the whole system was subjected to side-chain sampling and backbone minimization. The best energy conformation for each of the 100 independent simulations was used to generate a full atomic one-chain model by connecting the amino-terminal domain, the top of the helices, the extracellular loops, and the rest of the transmembrane domain. Each independent simulation typically lasted for 50 h. The health of the models was established by PROCHECK and WHAT_CHECK evaluations (Laskowski et al., 1993; Hooft et al., 1996).

Results

Probe Characterization. The Bpa^{5} probe was synthesized and purified as described under *Materials and Methods*, with its identity verified by matrix-assisted laser desorption/ionization–time-of-flight mass spectrometry. It bound to the secretin receptor saturably and specifically, with affinity slightly lower than that of natural secretin. This was demonstrated by its ability to compete for the binding of the secretin-like radioligand to the secretin receptor (Fig. 1) (K_i values: secretin, 2.7 ± 0.1 nM; Bpa^{5} probe, 7.7 ± 1.0 nM). This probe was also a full agonist, stimulating CHO-SecR cells to accumulate cAMP in a concentration-dependent manner, reaching a maximal level that was not different from that stimulated by natural secretin (Fig. 1). It had potency slightly lower than that of secretin (EC_{50} values: secretin, 0.06 ± 0.01 nM; Bpa^{5} probe, 0.13 ± 0.01 nM).

Photoaffinity Labeling of the Secretin Receptor. As shown in Fig. 2, the Bpa^{5} probe was able to covalently label the secretin receptor specifically and saturably, with the covalent labeling competed by secretin in a concentration-dependent manner (IC_{50} = 29.8 ± 6.1 nM). A single labeled band migrated at approximate M_r = 70,000 and shifted to approximate M_r = 42,000 after deglycosylation with endoglycosidase F, as expected for this receptor. No radioactive band was observed when non–receptor-bearing parental CHO cell membranes were treated the same way.

Identification of Labeled Receptor Region. CNBr was used to provide an initial indication of regions of labeling by the Bpa^{5} probe based on its ability to quantitatively cleave a protein at the carboxyl side of component Met residues. The secretin receptor contains nine Met residues; CNBr cleavage should, therefore, yield ten fragments ranging in molecular mass from 1 to 11 kDa, three of which contain sites of glycosylation (Fig. 3). As shown in Fig. 3, CNBr cleavage of the labeled native and deglycosylated secretin receptor bands resulted in both labeled fragments migrating at approximate M_r = 13,000. Taking into account the molecular mass of the attached probe (3228 Da) and the nonglycosylated nature of the labeled band, the receptor fragment labeled could be limited to two candidates. These were the fragments extending from TM3 to the third intracellular loop (Ala^{206}-Met^{299} highlighted in gray in Fig. 3) or extending from the third extracellular loop to the carboxyl-terminal tail (Glu^{345}-Ile^{429} highlighted in black in Fig. 3).

To definitively identify the region of labeling by the Bpa^{5} probe, two secretin receptor mutant constructs were prepared, H256M and L360M, with each introducing an additional Met residue within one of the candidate photolabeled fragments. Both receptor mutants bound secretin and signaled similarly to the wild-type receptor (Fig. 4). They were also specifically and saturably labeled with the Bpa^{5} probe (Fig. 5). CNBr cleavage of the labeled H256M receptor mutant yielded a labeled fragment that migrated at approximate M_r = 13,000 on a 10% NuPAGE gel, similar to that coming from the wild-type receptor. In contrast, CNBr cleavage of the labeled L360M receptor mutant yielded a much smaller fragment migrating at approximate M_r = 5000, consistent with the fragment Glu^{345}-Met^{360} including the labeled probe (Fig. 5). Taken together, these data indicate that the Glu^{345}-Ile^{429} fragment was the domain of labeling with the Bpa^{5} probe. Furthermore, this clearly established that the site of labeling was within the small segment be-

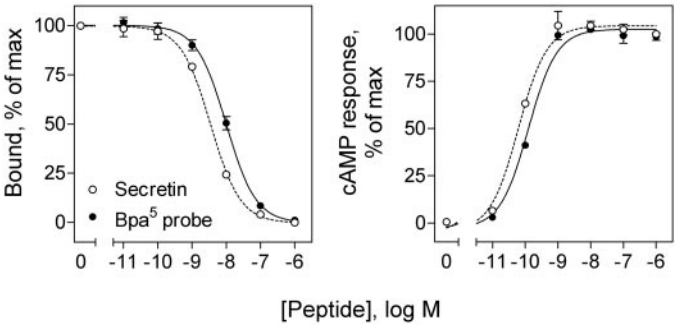

Fig. 1. Functional characterization of the Bpa^{5} probe. Left, competition-binding curves, reflecting the ability of increasing concentrations of secretin and the Bpa^{5} probe to displace the binding of the secretin-like radioligand to membranes from CHO-SecR cells. Values represent percentages of maximal saturable binding that were observed in the absence of competitor (3282 ± 45 cpm) and are expressed as means ± S.E.M. of duplicate data from three independent experiments. Right, intracellular cAMP responses to increasing concentrations of secretin and the Bpa^{5} probe in CHO-SecR cells. The basal level of intracellular cAMP was 1.3 ± 0.4 pmol/10^{6} cells, with the maximal stimulated levels reaching 198 ± 31 pmol/10^{6} cells. Values are expressed as means ± S.E.M. of data from three independent experiments performed in duplicate, with data normalized relative to the maximal response to secretin.

tween Glu^{345} and Leu^{360} that spans the third extracellular loop and TM7.

Identification of the Specific Site of Covalent Labeling. The radiochemically pure CNBr fragment (Glu^{345}-Ile^{429}) from the photoaffinity-labeled secretin receptor was used for manual Edman degradation sequencing to identify the specific residue labeled with the Bpa^{5} probe. Figure 6 shows the profiles of eluted radioactivity in which a peak was found in cycle 5, corresponding to the labeling of receptor residue Phe^{349} within the third extracellular loop.

Molecular Modeling. We recently reported models of secretin docked to the secretin receptor that are consistent with data from previous photoaffinity labeling and fluorescence resonance energy transfer experiments (Dong et al., 2007; Harikumar et al., 2007). We now incorporate substantial changes to the previous models that have resulted in significant improvements. For this, we have generated an up-to-date homology model of the rat secretin receptor amino-terminal domain, based on more recently deposited NMR constraints of the mouse CRF2β receptor (Grace et al., 2007)

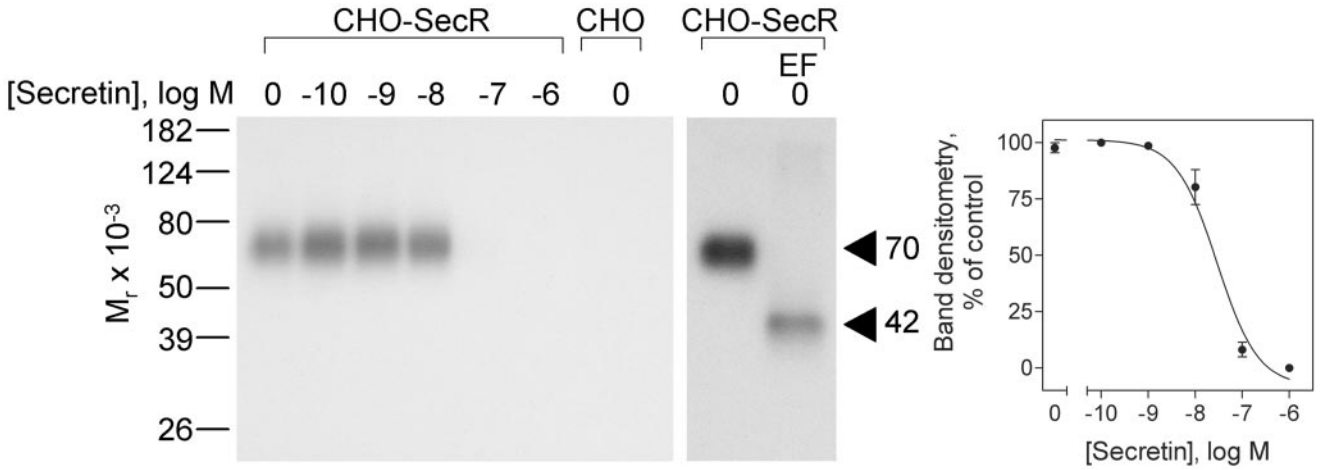

Fig. 2. Photoaffinity labeling of the secretin receptor. Left, representative autoradiographs of 10% SDS-polyacrylamide gels used to separate the products of photoaffinity labeling of plasma membranes from CHO-SecR cells with the Bpa^{5} probe in the presence of increasing concentrations of competing unlabeled secretin. As a control, absence of labeling of the nonreceptor-bearing CHO cell membranes in the absence of competitor is also shown. The labeled secretin receptor migrated at approximate M_r = 70,000 that shifted to approximate M_r = 42,000 after deglycosylation by endoglycosidase F (EF). No bands were detected in affinity-labeled non–receptor-bearing CHO cell membranes. Right, densitometric analyses of three similar independent experiments, with data points expressed as means ± S.E.M.

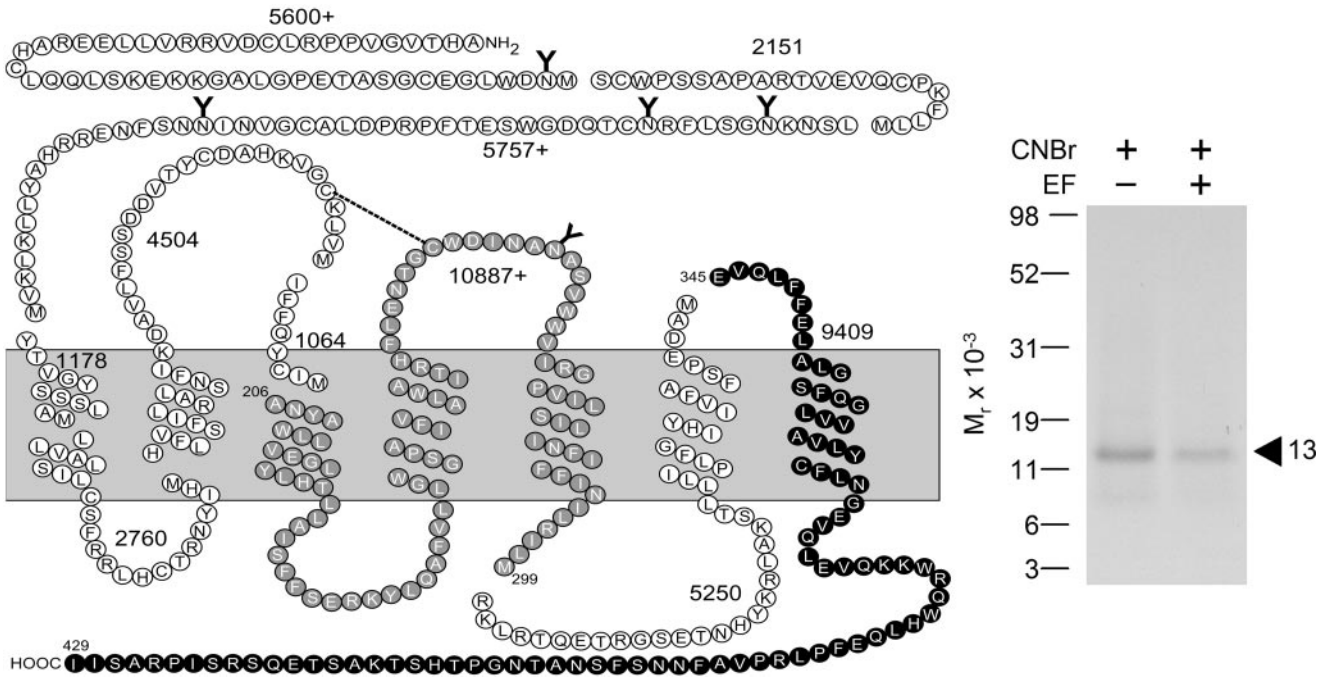

Fig. 3. CNBr cleavage of the labeled secretin receptor. Left, a diagram of the predicted sites of CNBr cleavage of the rat secretin receptor, along with the masses of protein cores of these fragments. Right, a representative autoradiograph of a 10% NuPAGE gel used to separate the products of CNBr cleavage of the secretin receptor labeled with the Bpa^{5} probe. CNBr cleavage of the labeled wild-type receptor yielded a fragment migrating at approximate M_r = 13,000. Cleavage of the labeled receptor deglycosylated with endoglycosidase F (EF) resulted in a fragment also migrating at approximate M_r = 13,000. These data are consistent with two candidates representing the fragments that include the second extracellular loop (gray circles) and the third extracellular loop and TM7 (bold circles).

and on the crystal structure of the amino terminus of the gastric inhibitory polypeptide receptor (Parthier et al., 2007). The latter provides key details of the structure of the distal ends of the amino terminus that had not been resolved in the NMR structures. We have also generated a refined homology model for the transmembrane helical bundle that incorporates the extracellular loop regions, explicitly allowing these regions to be flexible, starting with a structure based on the β2-adrenergic receptor (Cherezov et al., 2007). This provided a more open conformation of the extracellular loops than had been present previously with the rhodopsin structure. Given current concepts of the importance of these loops for peptide binding, this provided a useful starting point for modeling.

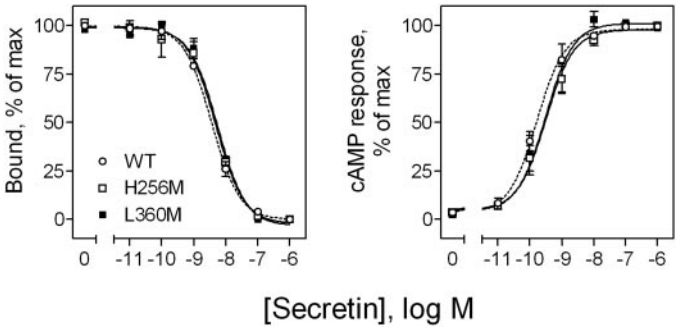

Fig. 4. Characterization of mutant secretin receptors. Shown are the abilities for the H256M and L360M mutant receptor constructs to bind secretin (left) and to stimulate intracellular cAMP accumulation in COS-1 cells (right). Data from three independent experiments performed in duplicate are illustrated as described in Fig. 1. WT, wild type.

We have docked secretin to 100 diverse conformations of the full receptor, using a series of experimentally derived constraints that are clearly described under *Materials and Methods*. The energetically most attractive models fell into two general groups of docked structures. These had the peptide docked either into a groove above the α-helical segment of the distal amino terminus of the receptor or below the same segment, situating the peptide adjacent to the transmembrane helical region of the receptor. The latter docking pose provided substantial contact between portions of the peptide and regions of the receptor core that have not been confirmed by photoaffinity labeling, provided more solvent accessibility than was observed in the fluorescence probe experiments (Harikumar et al., 2006), and placed the carboxyl terminus and mid region of the peptide closer to the receptor core than has been suggested by secretin receptor FRET studies (Harikumar et al., 2007). The models with the peptide in the groove above the helical segment, with the peptide amino terminus directed toward the receptor core region, were generally consistent with all previous experimental constraints. In careful quantitative evaluation of these models, the best model in this series, as determined by ICM global energetics is illustrated in Fig. 7. Table 1 demonstrates that the distances between the photolabile residues within secretin as docked in this model and the receptor residues labeled by each of the ten probes were fully consistent with the expectations of photoaffinity labeling in such experiments. This model also satisfied all of the FRET distances and all of the structure-activity considerations that currently exist (Harikumar et al., 2007).

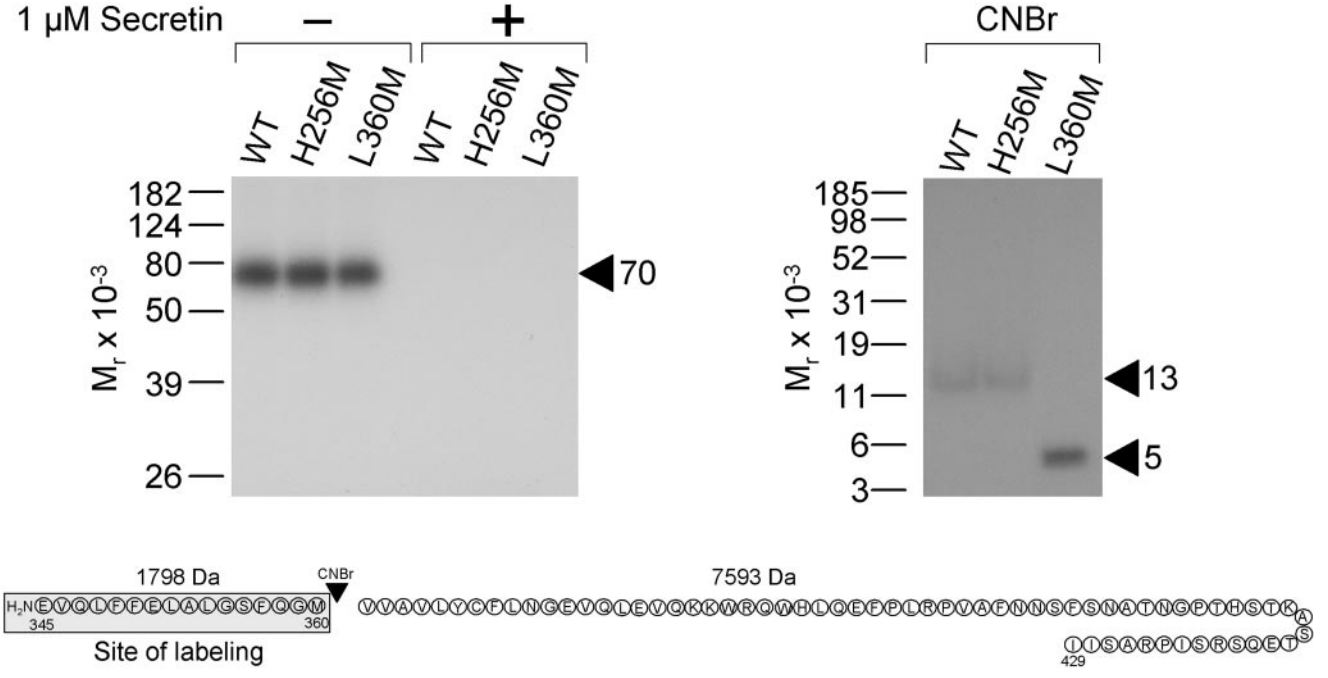

Fig. 5. Photoaffinity labeling and CNBr cleavage of the mutant secretin receptors. Left, a representative autoradiograph of a 10% gel used to separate the products of photoaffinity labeling of the H256M and L360M mutant secretin receptors by the Bpa^5 probe in the absence and presence of 1 μM competing secretin. Similar to experiments with wild-type receptor (WT), both receptor mutants were affinity-labeled saturably and specifically, with the labeled receptor migrating at approximate M_r = 70,000. Right, CNBr cleavage of the labeled receptor mutants. Like that of the wild-type receptor, the cleavage product of the labeled H256M receptor mutant migrated at approximate M_r = 13,000, whereas that from the L360M mutant receptor shifted its migration to approximate M_r = 5000. Bottom, theoretical sites and masses of expected fragments resulting from CNBr cleavage of the L360M receptor mutant (shown is the Glu^{345}-Ile^{429} fragment only). These data indicate that the region of labeling with the Bpa^5 probe was within the Glu^{345}-to-Leu^{360} fragment of the receptor.

Discussion

The major function of a membrane receptor is to bind an extracellular agonist ligand and to initiate intracellular signaling. The key for this to happen is the induction of a conformational change in the region of the receptor that interacts with its proximal effectors. For members of the G protein-coupled receptor superfamily, the helical bundle domain is critical for G protein coupling. This superfamily includes a remarkable spectrum of structurally diverse natural ligands, extending from small odorants and biogenic amines to small peptides, large glycoproteins, and even to viral particles. The organization of families of G protein-coupled receptors correlates nicely with these structural features of the natural ligands. Each family has evolved unique mechanisms for ligand binding and transmitting the effect of that binding to its helical bundle domain.

For the class II G protein-coupled receptors, it is now well established that ligand binding occurs primarily via the long and structurally complex, disulfide-bonded amino-terminal domain (Jüppner et al., 1994; Cao et al., 1995; Holtmann et al., 1995; Gourlet et al., 1996a,b; Dong et al., 2004b). Although we now have good insights into the structure of the amino-terminal domain of some of these receptors, based on the NMR structure of the amino terminus of the CRF2β receptor (Grace et al., 2004, 2007) and on the crystal structure of the amino terminus of the gastric inhibitory polypeptide receptor (Parthier et al., 2007), our insights into the helical bundle of receptors in this family are less clear. Based on primary sequence analysis and charge and hydrophobicity of conserved residues, the structure of the helical bundle of class II G protein-coupled receptors has been predicted to be quite distinct from that of rhodopsin and other class I G protein-coupled receptors (Frimurer and Bywater, 1999; Fredriksson et al., 2003; Foord et al., 2005).

In the current study, we have begun to refine our understanding of the helical bundle and core loop domains of the prototypic secretin receptor. These are the regions of this receptor that are essential for interaction with its amino-terminal domain that has been shown to be critical for the binding of natural ligands. Although we have a low resolution understanding of the relative orientation of the amino terminus with the helical bundle domain of this receptor (Dong et al., 2007; Harikumar et al., 2007), the number of experimentally derived constraints linking these two domains has been very limited. One such constraint includes the requirement for contiguity of the peptide backbone be-

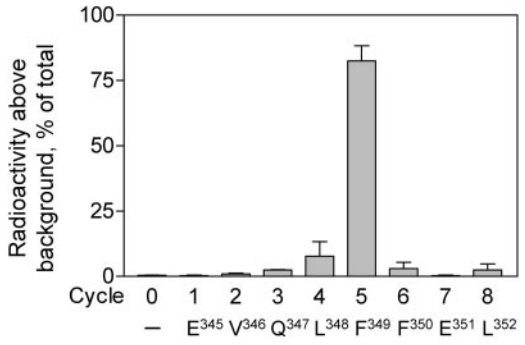

Fig. 6. Identification of the specific receptor residue covalently labeled by the Bpa[5] probe. Shown is the radioactive elution profile from Edman degradation sequencing of the Glu[345]-Ile[429] fragment from the wild-type secretin receptor labeled with the Bpa[5] probe. A peak eluted in radioactivity appeared in cycle 5, representing attachment of this probe to receptor residue Phe[349].

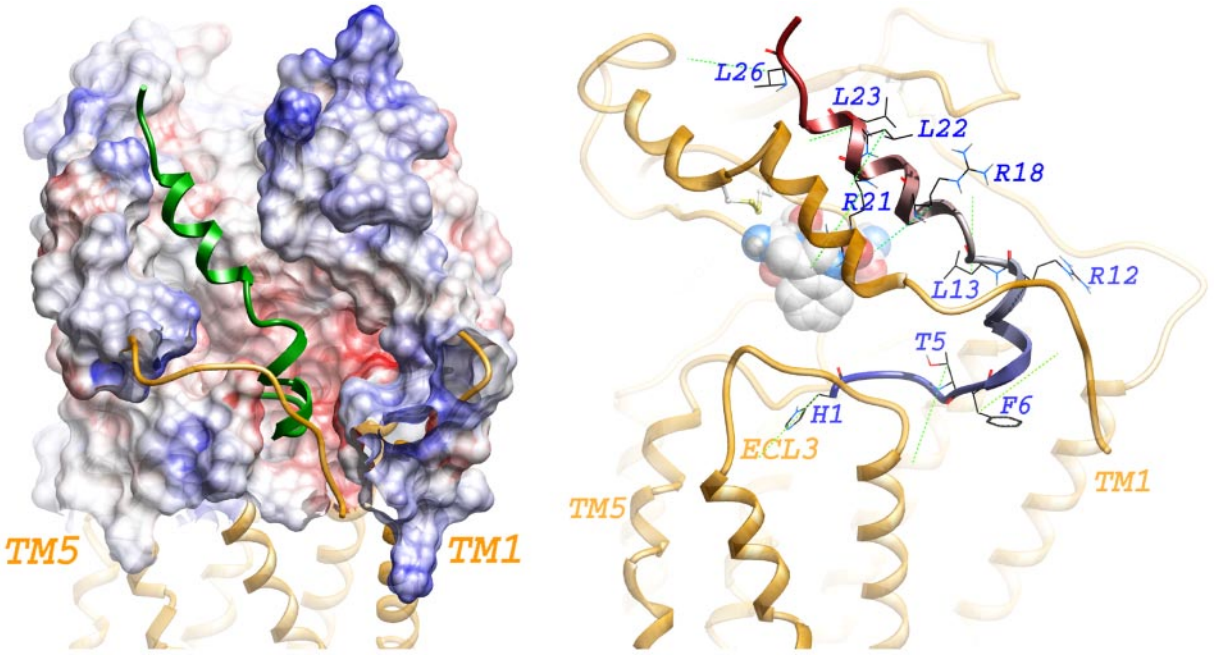

Fig. 7. Secretin receptor model. Shown is the best model of the 100 final models of secretin peptide docking. This model accommodates 10 photoaffinity labeling constraints and the three disulfide bonds shown to exist in the secretin receptor. Left, the full receptor is represented in orange ribbon. The secretin peptide is represented in green ribbon. Surface representation for the peptide binding surface is colored according to the electrostatic potential; blue, positive charge; red, negative charge. Right, the full receptor is represented in orange ribbon. The secretin peptide is colored blue-red from the amino terminus to the carboxyl terminus. The 10 photoaffinity labeling constraints are represented in green dotted lines. The cross-linked residues on the secretin peptide are represented by wire. The residues of the secretin peptide are labeled in blue. The proposed endogenous agonist sequence W[48]D[49]N[50] is shown in CPK representation. ECL, extracellular loop.

tween regions, with the carboxyl-terminal residue of the receptor amino terminus joined with the amino-terminal residue of the helical bundle domain, just above TM1. Another constraint that has been described for several members of this receptor family is the spatial approximation of the amino terminus of natural ligands with the third extracellular loop region above TM6 (Bisello et al., 1998; Dong et al., 2004a; Dong et al., 2004c). The most recent addition to this list is the spatial approximation of the endogenous agonist sequence within the amino terminus of the secretin receptor, WDN, with the same general region of the receptor (Dong et al., 2006).

Our previous report of a preliminary global model of secretin-occupied secretin receptor (Dong et al., 2007) used photoaffinity labeling data for residues approximated with residues within the receptor amino terminus, and other less quantitative insights, such as peptide structure-activity considerations and the spatial approximations described above. It is noteworthy that that preliminary model and its general orientation of the receptor amino terminus with the transmembrane helical bundle was further supported by fluorescence resonance energy transfer measurements between four residues distributed throughout the secretin pharmacophore and four residues within distinct regions of the secretin receptor (Dong et al., 2007; Harikumar et al., 2007). In that study, three quite distinct orientations of the amino terminus relative to the transmembrane helical bundle that were based on the existing proposals in the literature (Grace et al., 2004, 2007; Sun et al., 2007) were compared, and this orientation was determined to be the best. Although this approach was generally confirmatory, the relatively long distances and the bulky nature of the fluorophores used did not provide higher resolution refinement.

The current report adds more recently acquired residue-residue approximation constraints between residues at the amino terminus of secretin and the body of the secretin receptor (Dong et al., 2004a), as well as a new critical distance constraint between a photolabile residue in position five of the docked peptide and the third extracellular loop of the receptor. Because spatial constraints between a position along the secretin peptide and a residue in a region of the secretin receptor other than its amino terminus have been so rare, this provided key data that were particularly helpful in refining the current model. These data are analogous to the photoaffinity labeling of the third extracellular loop of the calcitonin receptor using a position eight calcitonin analog probe (Dong et al., 2004c). The currently proposed model uses recently released, better-refined NMR structures of the CRF2β receptor amino terminus (Grace et al., 2007) and an even better refined crystal structure of the amino terminus of the gastric inhibitory polypeptide receptor (Parthier et al., 2007), a more refined homology model of the helical bundle region using a recently published crystal structure of the human β-2-adrenergic receptor as template (Cherezov et al., 2007), as well as our first effort for refinement of extracellular loop domains of the secretin receptor.

There are three notable points to emphasize. First, in previous models the extracellular and intracellular loops of this receptor were either absent or were predefined through PDB search and were fixed during peptide docking. In the current model, the loops were fully flexible and sampled during simulation. Second, in previous models, the amino-terminal domain of the receptor was first connected to the transmembrane domain, and the secretin peptide was subsequently docked to one final conformation of the full receptor. As a result, the amino-terminal domain was virtually fixed during peptide docking, thus limiting the peptide docking site available in the model. In the current model, 10,000 initial conformations of the full receptor were generated, 100 of which were selected for subsequent peptide docking on the basis of identification of a viable peptide-binding site using the ICM-PocketFinder algorithm (An et al., 2005). This drastically increases the sampling space. Finally, because of the nature of Monte Carlo simulation in internal coordinate mechanics, which moves the atoms downstream of the sampled variable, the highly flexible distal end of the amino terminus was not efficiently sampled in previous models. In the current model, the distal end of the amino terminus was added in the second stage of the simulation and was sampled independently, using a reverse Monte Carlo procedure that moves the atoms upstream of the sampled variable. This resulted in a much more efficient sampling of the distal end of the amino terminus, reflected in better-satisfied distance restraints to this region. The final distances between the C_β atoms of the cross-linked residues in secretin and in the secretin receptor for the best model in the series were all between 6.7 and 9.3 Å, well within the reach of any of the photoaffinity labeling groups employed in the specific probes that have been used. This allows for the rotational flexibility of the side chains involved, as well as for the 3.1-Å limit that has been proposed to achieve efficient cross-linking with analogous probes.

In the current best model, secretin lies in a binding cleft within the secretin receptor amino terminus with the peptide amino terminus directed toward the receptor body. Within this cleft, the carboxyl-terminal third of the peptide is in an α-helical conformation that is parallel to an α helix within the receptor. Multiple photoaffinity labeling constraints support a helix-helix interaction for this region (Dong et al., 1999b, 2000, 2002, 2007). This is followed by the mid-region of the peptide that has sites of photoaffinity labeling that alternates between the distal amino terminus and other portions of the receptor amino terminus. This is consistent with the mid-region and carboxyl terminus of secretin being relatively protected from quenching by hydrophilic agents, as demonstrated in fluorescence studies (Harikumar et al., 2006). The distal amino terminus of the peptide is directed toward the third extracellular loop of the receptor, with two distinct photoaffinity labeling constraints (Dong et al., 2004a) that support a terminal loop structure at the end of

TABLE 1
C_β distances between cross-linked residues in secretin and the secretin receptor of the best model in the series

Secretin Residue	Secretin Receptor Residue	Distances
		Å
His^{1}	Phe^{338}	9.3
Thr^{5}	Phe^{349}	8.4
Leu^{13}	Val^{103}	8.4
Leu^{26}	Leu^{36}	8.0
Phe^{6}	Val^{4}	9.3
Arg^{12}	Val^{6}	8.6
Arg^{18}	Arg^{14}	6.7
Arg^{21}	Arg^{15}	8.4
Leu^{22}	Leu^{17}	7.7
Leu^{23}	Arg^{21}	8.3

the helical portion of the peptide. As we learned from the fluorescence studies, the distal amino terminus of secretin is highly exposed to the solvent, lying between the protection of the binding cleft and the receptor body.

We believe that the currently proposed model of secretin docked to its receptor represents the most comprehensive and best model that has yet been reported, and as such will enhance the design of future experiments that will be critical for our understanding of the structure and mechanism of activation of this receptor. Nonetheless, there remain critical areas for future improvement of this model that include refinement of the helical bundle to account for the predicted differences between class II and class I receptor structure, improved modeling of the extracellular loops of the receptor that is dependent on final positioning of the transmembrane helices and additional constraints on the positioning of the receptor amino terminus relative to the receptor core.

Acknowledgments

We acknowledge the contributions of Dr. K. Hosohata in the preliminary studies with this photolabile probe and the excellent technical assistance of L. A. Bruins and R. M. Happs.

References

Abagyan R and Totrov M (1994) Biased probability Monte Carlo conformational searches and electrostatic calculations for peptides and proteins. *J Mol Biol* **235:**983–1002.

Abagyan R, Totrov M, and Kuznetsov D (1994) Icm—a new method for protein modeling and design—applications to docking and structure prediction from the distorted native confirmation. *J Comput Chem* **15:**488–506.

An J, Totrov M, and Abagyan R (2005) Pocketome via comprehensive identification and classification of ligand binding envelopes. *Mol Cell Proteomics* **4:**752–761.

Bisello A, Adams AE, Mierke DF, Pellegrini M, Rosenblatt M, Suva LJ, and Chorev M (1998) Parathyroid hormone-receptor interactions identified directly by photocross-linking and molecular modeling studies. *J Biol Chem* **273:**22498–22505.

Cao YJ, Gimpl G, and Fahrenholz F (1995) The amino-terminal fragment of the adenylate cyclase activating polypeptide (PACAP) receptor functions as a high affinity PACAP binding domain. *Biochem Biophys Res Commun* **212:**673–680.

Cherezov V, Rosenbaum DM, Hanson MA, Rasmussen SG, Thian FS, Kobilka TS, Choi HJ, Kuhn P, Weis WI, Kobilka BK, et al. (2007) High-resolution crystal structure of an engineered human beta2-adrenergic G protein-coupled receptor. *Science* **318:**1258–1265.

Clore GM, Nilges M, Brunger A, and Gronenborn AM (1988) Determination of the backbone conformation of secretin by restrained molecular dynamics on the basis of interproton distance data. *Eur J Biochem* **171:**479–484.

Dong M, Asmann YW, Zang M, Pinon DI, and Miller LJ (2000) Identification of two pairs of spatially approximated residues within the carboxyl terminus of secretin and its receptor. *J Biol Chem* **275:**26032–26039.

Dong M, Lam PC, Gao F, Hosohata K, Pinon DI, Sexton PM, Abagyan R, and Miller LJ (2007) Molecular approximations between residues 21 and 23 of secretin and its receptor: development of a model for peptide docking with the amino terminus of the secretin receptor. *Mol Pharmacol* **72:**280–290.

Dong M, Li Z, Pinon DI, Lybrand TP, and Miller LJ (2004a) Spatial approximation between the amino terminus of a peptide agonist and the top of the sixth transmembrane segment of the secretin receptor. *J Biol Chem* **279:**2894–2903.

Dong M, Li Z, Zang M, Pinon DI, Lybrand TP, and Miller LJ (2003) Spatial approximation between two residues in the mid-region of secretin and the amino terminus of its receptor. Incorporation of seven sets of such constraints into a three-dimensional model of the agonist-bound secretin receptor. *J Biol Chem* **278:**48300–48312.

Dong M, Pinon DI, Asmann YW, and Miller LJ (2006) Possible endogenous agonist mechanism for the activation of secretin family G protein-coupled receptors. *Mol Pharmacol* **70:**206–213.

Dong M, Pinon DI, Cox RF, and Miller LJ (2004b) Importance of the amino terminus in secretin Family G protein-coupled receptors: intrinsic photoaffinity labeling establishes initial docking constraints for the calcitonin receptor. *J Biol Chem* **279:**1167–1175.

Dong M, Pinon DI, Cox RF, and Miller LJ (2004c) Molecular approximation between a residue in the amino-terminal region of calcitonin and the third extracellular loop of the class B G protein-coupled calcitonin receptor. *J Biol Chem* **279:**31177–31182.

Dong M, Wang Y, Hadac EM, Pinon DI, Holicky E, and Miller LJ (1999a) Identification of an interaction between residue 6 of the natural peptide ligand and a distinct residue within the amino-terminal tail of the secretin receptor. *J Biol Chem* **274:**19161–19167.

Dong M, Wang Y, Pinon DI, Hadac EM, and Miller LJ (1999b) Demonstration of a direct interaction between residue 22 in the carboxyl-terminal half of secretin and the amino-terminal tail of the secretin receptor using photoaffinity labeling. *J Biol Chem* **274:**903–909.

Dong M, Zang M, Pinon DI, Li Z, Lybrand TP, and Miller LJ (2002) Interaction among four residues distributed through the secretin pharmacophore and a focused region of the secretin receptor amino terminus. *Mol Endocrinol* **16:**2490–2501.

Foord SM, Bonner TI, Neubig RR, Rosser EM, Pin JP, Davenport AP, Spedding M, and Harmar AJ (2005) International Union of Pharmacology. XLVI. G protein-coupled receptor list. *Pharmacol Rev* **57:**279–288.

Fredriksson R, Lagerstrom MC, Lundin LG, and Schioth HB (2003) The G-protein-coupled receptors in the human genome form five main families. Phylogenetic analysis, paralogon groups, and fingerprints. *Mol Pharmacol* **63:**1256–1272.

Frimurer TM and Bywater RP (1999) Structure of the integral membrane domain of the GLP1 receptor. *Proteins* **35:**375–386.

Gardner JD, Conlon TP, Beyerman HC, and Van Zon A (1977) Interaction of synthetic 10-tyrosyl analogues of secretin with hormone receptors on pancreatic acinar cells. *Gastroenterology* **73:**52–56.

Gourlet P, Vilardaga JP, De Neef P, Vandermeers A, Waelbroeck M, Bollen A, and Robberecht P (1996a) Interaction of amino acid residues at positions 8–15 of secretin with the N-terminal domain of the secretin receptor. *Eur J Biochem* **239:**349–355.

Gourlet P, Vilardaga JP, De Neef P, Waelbroeck M, Vandermeers A, and Robberecht P (1996b) The C-terminus ends of secretin and VIP interact with the N-terminal domains of their receptors. *Peptides* **17:**825–829.

Grace CR, Perrin MH, DiGruccio MR, Miller CL, Rivier JE, Vale WW, and Riek R (2004) NMR structure and peptide hormone binding site of the first extracellular domain of a type B1 G protein-coupled receptor. *Proc Natl Acad Sci U S A* **101:**12836–12841.

Grace CR, Perrin MH, Gulyas J, Digruccio MR, Cantle JP, Rivier JE, Vale WW, and Riek R (2007) Structure of the N-terminal domain of a type B1 G protein-coupled receptor in complex with a peptide ligand. *Proc Natl Acad Sci U S A* **104:**4858–4863.

Hadac EM, Ghanekar DV, Holicky EL, Pinon DI, Dougherty RW, and Miller LJ (1996) Relationship between native and recombinant cholecystokinin receptors: role of differential glycosylation. *Pancreas* **13:**130–139.

Harikumar KG, Hosohata K, Pinon DI, and Miller LJ (2006) Use of probes with fluorescence indicator distributed throughout the pharmacophore to examine the peptide agonist-binding environment of the family B G protein-coupled secretin receptor. *J Biol Chem* **281:**2543–2550.

Harikumar KG, Lam PC, Dong M, Sexton PM, Abagyan R, and Miller LJ (2007) Fluorescence resonance energy transfer analysis of secretin docking to its receptor: Mapping distances between residues distributed throughout the ligand pharmacophore and distinct receptor residues. *J Biol Chem* **282:**32834–32843.

Holtmann MH, Ganguli S, Hadac EM, Dolu V, and Miller LJ (1996) Multiple extracellular loop domains contribute critical determinants for agonist binding and activation of the secretin receptor. *J Biol Chem* **271:**14944–14949.

Holtmann MH, Hadac EM, and Miller LJ (1995) Critical contributions of amino-terminal extracellular domains in agonist binding and activation of secretin and vasoactive intestinal polypeptide receptors. Studies of chimeric receptors. *J Biol Chem* **270:**14394–14398.

Hooft RWW, Vriend G, Sander C, and Abola EE (1996) Errors in protein structures. *Nature* **381:**272.

Ji Z, Hadac EM, Henne RM, Patel SA, Lybrand TP, and Miller LJ (1997) Direct identification of a distinct site of interaction between the carboxyl-terminal residue of cholecystokinin and the type A cholecystokinin receptor using photoaffinity labeling. *J Biol Chem* **272:**24393–24401.

Jüppner H, Schipani E, Bringhurst FR, McClure I, Keutmann HT, Potts JT Jr., Kronenberg HM, Abou-Samra AB, Segre GV, and Gardella TJ (1994) The extracellular amino-terminal region of the parathyroid hormone (PTH)/PTH-related peptide receptor determines the binding affinity for carboxyl-terminal fragments of PTH-(1–34). *Endocrinology* **134:**879–884.

Kofod H (1991) Synthesis of biologically active porcine secretin and [ITyr10] porcine secretin. *Int J Pept Protein Res* **37:**185–190.

Laemmli UK (1970) Cleavage of structural proteins during the assembly of the head of bacteriophage T4. *Nature* **227:**680–685.

Laskowski RA, Macarthur MW, Moss DS, and Thornton JM (1993) Procheck—a program to check the stereochemical quality of protein structures. *J Appl Crystallogr* **26:**283–291.

Metropolis N, Rosenbluth AW, Rosenbluth MN, Teller AH, and Teller E (1953) Equation of state calculations by fast computing machines. *J Chem Phys* **21:**1087–1092.

Munson PJ and Rodbard D (1980) Ligand: a versatile computerized approach for characterization of ligand-binding systems. *Anal Biochem* **107:**220–239.

Parthier C, Kleinschmidt M, Neumann P, Rudolph R, Manhart S, Schlenzig D, Fanghanel J, Rahfeld JU, Demuth HU, and Stubbs MT (2007) Crystal structure of the incretin-bound extracellular domain of a G protein-coupled receptor. *Proc Natl Acad Sci U S A* **104:**13942–13947.

Pearson RK, Miller LJ, Hadac EM, and Powers SP (1987) Analysis of the carbohydrate composition of the pancreatic plasmalemmal glycoprotein affinity labeled by short probes for the cholecystokinin receptor. *J Biol Chem* **262:**13850–13856.

Powers SP, Pinon DI, and Miller LJ (1988) Use of *N,O*-bis-Fmoc-D-Tyr-ONSu for introduction of an oxidative iodination site into cholecystokinin family peptides. *Int J Pept Protein Res* **31:**429–434.

Sanger F, Nicklen S, and Coulson AR (1977) DNA sequencing with chain-terminating inhibitors. *Proc Natl Acad Sci U S A* **74:**5463–5467.

Sun C, Song D, Davis-Taber RA, Barrett LW, Scott VE, Richardson PL, Pereda-Lopez A, Uchic ME, Solomon LR, Lake MR, et al. (2007) Solution structure and mutational analysis of pituitary adenylate cyclase-activating polypeptide binding to the extracellular domain of PAC1-RS. *Proc Natl Acad Sci U S A* **104:**7875–7880.

Ulrich CD 2nd, Holtmann M, and Miller LJ (1998) Secretin and vasoactive intestinal

peptide receptors: members of a unique family of G protein-coupled receptors. *Gastroenterology* **114:**382–397.
Ulrich CD 2nd, Pinon DI, Hadac EM, Holicky EL, Chang-Miller A, Gates LK, and Miller LJ (1993) Intrinsic photoaffinity labeling of native and recombinant rat pancreatic secretin receptors. *Gastroenterology* **105:**1534–1543.
Zang M, Dong M, Pinon DI, Ding XQ, Hadac EM, Li Z, Lybrand TP, and Miller LJ (2003) Spatial approximation between a photolabile residue in position 13 of secretin and the amino terminus of the secretin receptor. *Mol Pharmacol* **63:**993–1001.

Address correspondence to: Dr. Laurence J. Miller, Mayo Clinic, 13400 East Shea Blvd., Scottsdale, AZ 85259. E-mail: miller@mayo.edu